Direct Measurement of the Millimeter Wave Phase Singularity with Helical Wavefront using Heterodyne Detection System at Two Spatial Points*)

Yuki GOTO, Shin KUBO[1)], Toru Ii TSUJIMURA and Toru KOBAYASHI[2)]

National Institute for Fusion Science, National Institutes of Natural Sciences, Toki 509-5292, Japan
[1)]*College of Engineering, Chubu University, Kasugai 487-8501, Japan*
[2)]*Department of Applied Energy, Nagoya University, Nagoya 464-8603, Japan*

(Received 27 December 2021 / Accepted 27 January 2022)

In this paper, we measured the one-dimensional phase and polarization structure of a millimeter-wave with a helical wavefront (vortex beam) using a simultaneous heterodyne detection system at two spatial points. This is a novel approach, and it provides us with the relative phase of the vortex beam. We measured the phase discontinuity of the vortex beam by scanning the one-dimensional path where an antenna passes through the optical axis. It was found that relative phases gradually increase or decrease when the antenna does not pass through the optical axis. Additionally, we measured polarization parameters, which were indefinite near the optical axis. In other words, the optical axis of the vortex beam is a singular point about the phase.

Keywords: vortex beam, helical wavefront, phase singularity, heterodyne detection system, millimeter-wave

DOI: 10.1585/pfr.17.2401007

1. Introduction

A Laguerre Gaussian (LG) mode is the paraxial solution of the wave equation in a cylindrical coordinate system. It is also called an optical vortex [1]. The equiphase front of an optical vortex has a helical phase structure, which is characterized by an integer number called the Topological Charge (TC). Furthermore, an optical vortex has a donut-shaped intensity distribution, which means zero intensity on the optical axis.

Recently, studies have been conducted on applying a millimeter-wave with a helical wavefront (vortex beam) to fusion plasma. This is because it has been theoretically shown that higher harmonics radiation from an electron in the spiral motion has vortex characteristics. Further, it has also been recognized that an electron cyclotron motion and its emission are closely related to the vortex beam [2–5]. Interestingly, it was numerically shown that there is a unique propagation property of the vortex beam in a magnetized plasma [6]. That suggests part of the vortex beam can penetrate the plasma cutoff region, and we may establish a new heating method of the over-dense plasma using the vortex beam.

To experimentally demonstrate the plasma heating by the vortex beam, a spiral mirror has been successfully developed to generate the vortex beam in the millimeter wave regime. This is a passive optical element to produce a vortex beam by conversion from the Gaussian beam [7]. Additionally, to identify the vortex beam in the millimeter-wave regime, we established a measurement method of the vortex beam using a triangular aperture [7]. We used the aperture for measuring the vortex beam, since the characteristic diffraction pattern can be obtained based on the phase structure of the vortex beam.

However, it is necessary to develop a new measurement system for the vortex beam because of the difficulty in the alignment. To obtain characteristic diffraction patterns clearly, we realize an alignment where the bright ring is slightly larger than the inscribed circle of the triangular aperture. Moreover, even if the difference in wavelength between the center of gravity of the triangular aperture and optical axis of the vortex beam is half, the diffraction patterns are uneven. Then, the identification of the vortex beam becomes difficult.

Therefore, we developed a new measurement system for detecting a vortex beam in a millimeter-wave regime using the heterodyne detection method arranged at two spatial points. The system has two receiving antennas: one is fixed with phase ϕ_f and the other is movable with phase ϕ_m one-dimensionally. Thus, the system provides us with the relative phase of the vortex beam $\phi_\mathrm{m} - \phi_\mathrm{f}$. Since the phase structure of the vortex beam has a spatial dependence on the azimuthal angle, and the optical axis is the singular point about a phase, the relative phase must have a phase discontinuity at the optical axis. Additionally, having a phase discontinuously at the optical axis, means that the electric field around the optical axis is rationally distributed. Therefore, it should also be indefinite for polar-

author's e-mail: goto.yuki@nifs.ac.jp
*) This article is based on the presentation at the 30th International Toki Conference on Plasma and Fusion Research (ITC30).

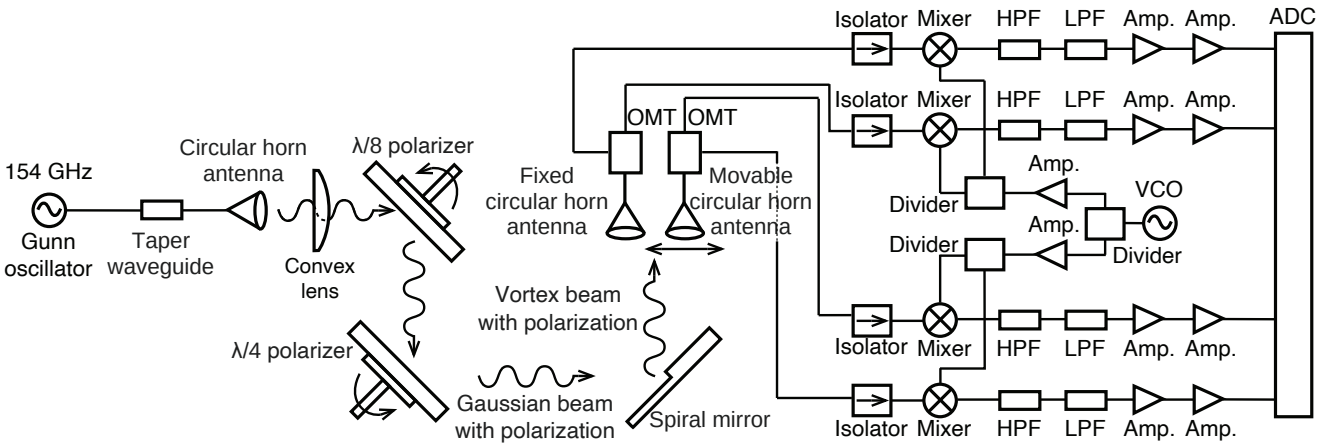

Fig. 1 Experimental setup for measuring phase singularity using heterodyne detection system at two spatial points. One is fixed antenna, the other is movable antenna one-dimensionally. Decomposed signals are digitized by ADC after frequency down converted to IF signal by mixer. In this system, voltage controlled oscillator (VCO) signal is commonly used.

ization at the point of using a heterodyne detection system with an Orthomode Transducer (OMT). If we can detect the phase discontinuity across the optical axis directly, we can identify the vortex beam with a donut-shaped intensity distribution.

This paper is composed of four sections. In Section 2, the experimental setup of the new measurement system for the vortex beam and development of the key components are briefly described. In Section 3, experimental results of the vortex beam measured using two spatial heterodyne detection systems are discussed. The summary of this paper is provided in Section 4.

2. Experimental Setup

Figure 1 shows the experimental setup of the new measurement system for the vortex beam. In the experiment, the heterodyne detection system is arranged at two spatial points. One is fixed with the phase ϕ_{f}, and the other is movable with the phase ϕ_{m}, one-dimensionally. Therefore, it is possible to detect the relative phase of the vortex beam $\phi_{\mathrm{m}} - \phi_{\mathrm{f}}$ by measuring at two spatial points. The injection beam from the 154 GHz Gunn oscillator is focused by the convex lens and converted to a Gaussian beam with arbitrary polarization using a set of polarizers. This beam is reflected by a spiral mirror to generate a polarized vortex beam. Additionally, since the heterodyne system in this experiment can decompose the beam with an arbitrary polarization state into orthogonal components using the OMT, the measurement of one-dimensional polarization parameters of the vortex beam can be obtained. Each orthogonal component is converted to an intermediate frequency (IF) signal using the heterodyne detection system, and then digitized by an analog-to-digital converter (ADC). Since the back side of the spiral mirror is fabricated to form a plane mirror, the experiment can be performed by turning over the mirror in cases of TC = 1 and TC = 0.

The following describes development of the OMT and

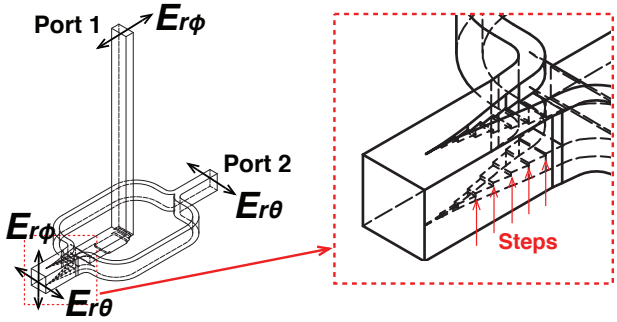

Fig. 2 Internal structure of OMT with double ridge. Input port has square waveguide, output ports have rectangular waveguide. $E_{r\phi}$ component is guided to port 1, $E_{r\theta}$ component is guided to port 2, respectively.

polarizers, which are critical components of this experiment.

2.1 Development of Orthomode Transducer

To measure the polarization state of a wave by the heterodyne detection system, it is necessary to install an OMT on the waveguide circuit. The OMT is the key waveguide component that separates the input beam into orthogonally linear polarized components. Thus, we designed and manufactured the step taper double-ridged OMT, as shown in Fig. 2. This is the first OMT insourced at the National Institute for Fusion Science (NIFS). This OMT design is based on the report by Asayama *et al.* [8], which originally had a smooth taper structure at the decomposing section. However, our OMT has a step taper structure that overcomes the difficulty of the machining process. Moreover, it is for the D-band expansion (110 - 170 GHz) from a 70 - 120 GHz, 1.65 × 1.65 mm square waveguide for the input, and 1.65 × 0.825 (WR-06) rectangular waveguides for the output.

Figure 3 shows the results of the performance test of

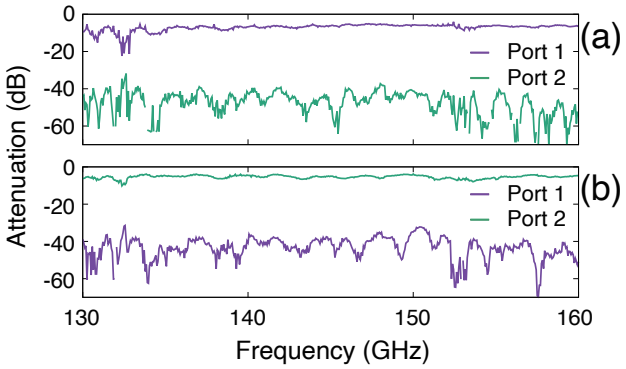

Fig. 3 Frequency dependence of separation performance of OMT we developed. (a): If input component has only $E_{r\phi}$. (b): If input component has only $E_{r\theta}$.

the OMT. The horizontal axis represents the frequency of the input signal and the vertical axis represents common logarithms of output power P_{out} over input power P_{in} at each port, which indicates the attenuation rate A_p (dB): $A_p = 10\log_{10}\left(\frac{P_{\text{out}}}{P_{\text{in}}}\right)$. The input signal is generated by a synthesizer (model MG37022A by Anritsu) while changing from 16 GHz to 20 GHz. Then, the signal frequency is changed by 130 - 160 GHz, using multipliers with a factor of four and two. A few mW, is injected into the OMT via the taper transit between the rectangular and square. Furthermore, we measured two cases where the electric field of the input signal had only an $E_{r\phi}$ direction and only an $E_{r\theta}$ direction, which was lineally polarized. Then, the orthogonally decomposed signals' power was revealed at port 1 and 2 by a detector. As can be seen, our OMT had over 40 dB of separation. Thus, we could successfully develop the OMT in the D-band and even the OMT had no smooth taper structure.

2.2 Development of polarizers

To produce the vortex beam in a millimeter-wave regime with arbitrary polarization, it is necessary to control the ratio and phase difference, regarding orthogonal field components, by a polarizer. In this study, polarization control was performed by using a polarizer specialized for 154 GHz (D-band) with a rounded shape at the edge of the period groove surface, which was originally designed for 82.7 GHz by Ii *et al* for a mega-watt long-pulse millimeter-wave transmission line of the electron cyclotron resonance heating system in the large helical device [9]. As shown in Fig. 4 (a), we designed the polarizer composed of two types of grating mirrors, which are $\lambda/8$-type and $\lambda/4$-type grating mirrors. Since the injection angle is considered at angle 45 degrees, groove depths are set to be $\lambda/8/\cos 45 \simeq 0.4605\lambda$ and $\lambda/4/\cos 45 \simeq 0.7069\lambda$. The period of the groove p is selected as $p = 0.9\,\text{mm} < \lambda/2$ so that higher order diffraction is suppressed. At a grating mirror of $\lambda/4$, the rotation angle of the polarization α can be roughly controlled, while the ellipticity of the polarization β can be controlled on the grating mirror at $\lambda/8$ (shown in Fig. 4 (b)). Thus, by rotating the polarizers, we can produce a wave with arbitrary polarization status.

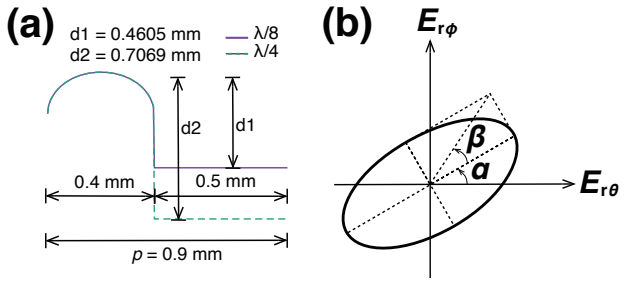

Fig. 4 (a): Shape of groove of grating mirrors. (b): Definition of polarization parameters; α and β.

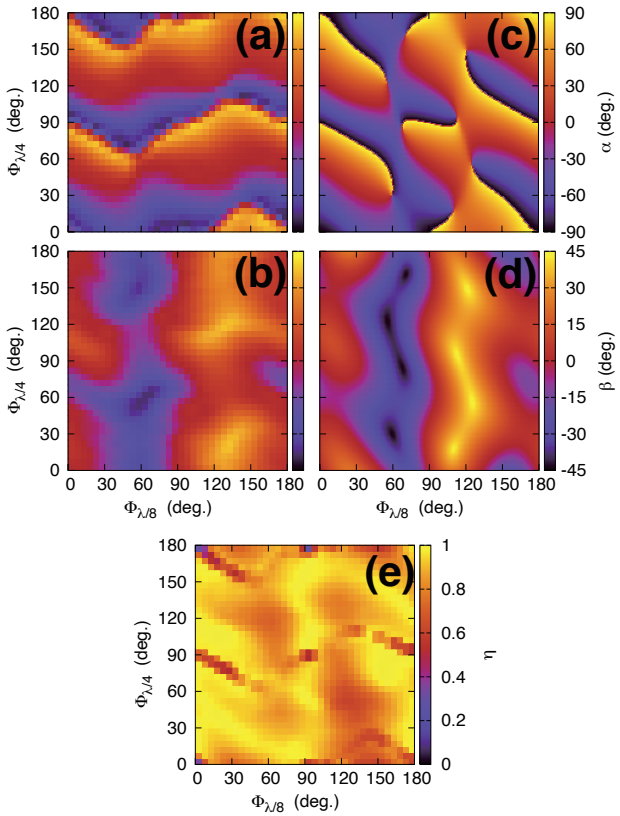

Fig. 5 Polarization parameters ($\alpha \cdot \beta$) depending on rotation angles $\Phi_{\lambda/4}$ and $\Phi_{\lambda/8}$ for grating mirrors. (a) and (b) are experimental results. (c) and (d) numerical calculation results based on integral method. (e) is polarization purity between experimental results and numerical calculation results.

Figures 5 (a) to (d) show experimental and numerical calculation results of polarization parameters (α,β), depending on the rotation angle of the grating mirrors. As a result, these experimental results were well compatible with the calculation results and reproduce that of Ii [9]. Since these grating mirrors have the same groove shape based on Ii's result, the dependence of the polarization parameters was the same, even if we used a different fre-

quency. Additionally, as shown in Fig. 5 (e), polarization purity (coincidence degree) between experimental and numerical calculation results was more than 80 % at almost all rotation angles. This numerical calculation is based on the integral method well known as the vector theories of the grating mirror [9–12].

3. Vortex Beam Measurement Experiment

Consequently, we can generate a beam with an arbitrary polarization in the D-band, and we can identify the polarization parameters by dividing the receiving signal into two orthogonal components using our OMT. In this section, a beam with the polarization $(\alpha, \beta) = (60, 10)$ is injected into a spiral mirror to generate a vortex beam with an arbitrary polarization. Here the polarization parameters are chosen as the polarization purity becomes high with the rotation angles $(\Phi_{\lambda/4}, \Phi_{\lambda/8}) = (120, 10)$ in Fig. 5. Furthermore, the cross section of the beam is one-dimensionally measured by the heterodyne detection system with a movable antenna.

Figures 6 (a) and (b) show the intensity distribution of the beam with TC = 0 and TC = 1, measured by a two-dimensional camera (terahertz camera model T30/64/64 produced by Terasense Group Inc.), which is set at the same place as the antenna of the heterodyne detection system. Notably, in the case of TC = 0, the intensity distribution has a peak on the optical axis. However, in the case of TC = 1, the intensity distribution is donut-shaped without an intensity peak on the optical axis. Figures 6 (c) to (f) show the numerical calculation results of the intensity and phase distribution. Meanwhile, (c) and (e) are for TC = 0, (d) and (f) are for TC = 1. In this calculation, the beam is considered as a plane wave which has no curvature of the wavefront. Therefore, when TC = 0, there is no phase structure in the azimuthal direction at the arbitrary beam cross section. However, when TC = 1, the phase continuously changes in the azimuthal direction. In the experiments, the fixed antenna is located on the point shown in Figs. 6 (a) and (b), and the movable antenna is scanned one-dimensionally from left to right, shown in Figs. 6 (a) and (b) at three paths. The center path is passing through the optical axis, and top and bottom paths are not passing through it.

Figure 7 shows a comparison of one-dimensional intensity distribution between the calculation and experimental results, measured by the heterodyne detection system at each scan path. From (a) to (c) are numerical calculation results, while from (d) to (f) are experimental ones. It is easy to see that in the case of TC = 1 at every path, the distribution has an intensity drop near the optical axis, which is a characteristic of the vortex beam. In the case of TC = 0 at every path, the intensity distribution has a peak near the optical axis, which is characteristic of the Gaussian beam. Here, it is noteworthy that the size of the antenna cross section is considered in the calculation and one data point is based on the summation of the electric field over the antenna cross section.

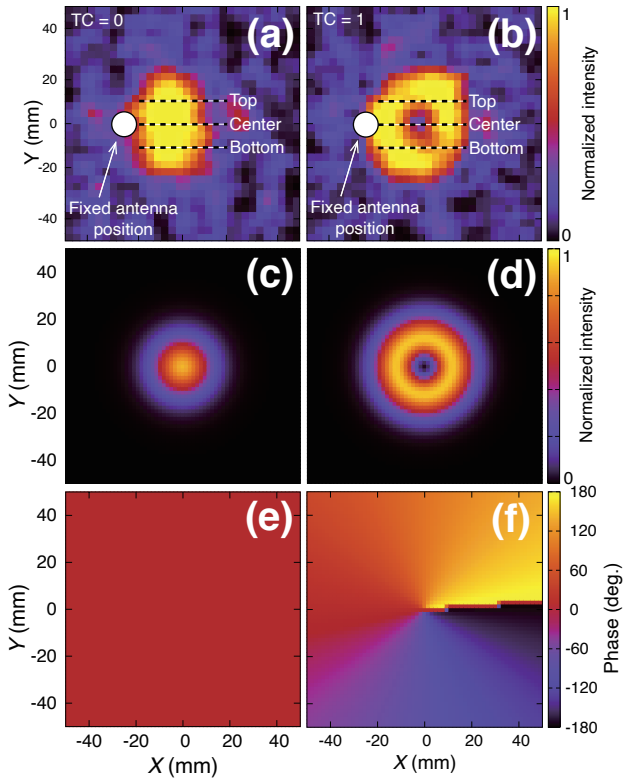

Fig. 6 (a) and (b) are intensity distribution taken by two dimensional camera. Fixed antenna is located at white circle, movable antenna is scanned on black dot-line path. (c) and (d) are intensity distribution, (e) and (f) are phase distribution, which are calculated by using LG mode with TC = 0 and TC = 1.

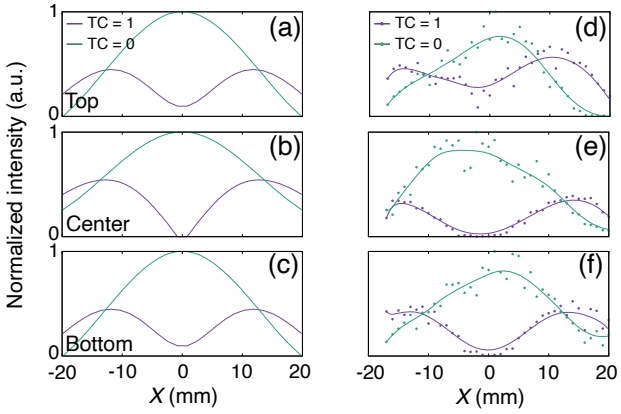

Fig. 7 One-dimensional intensity distribution measured by heterodyne detection system at each scan path. From (a) to (c) are numerical calculation, (d) to (f) are experimental results. Solid lines are drawn by Bézier interpolation.

Figure 8 shows a comparison of the relative phase variation between calculation and experimental results. From (a) to (c) are numerical calculations and from (d) to

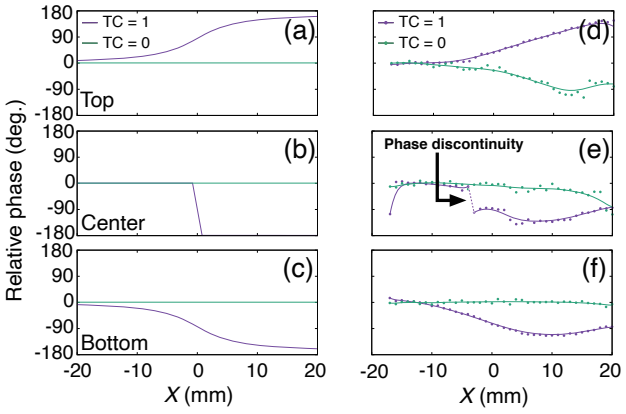

Fig. 8 Variation of the relative phase depending on the position X at each scan path. From (a) to (c) are numerical calculation, (d) to (f) are experimental results. Solid lines are drawn by Bézier interpolation.

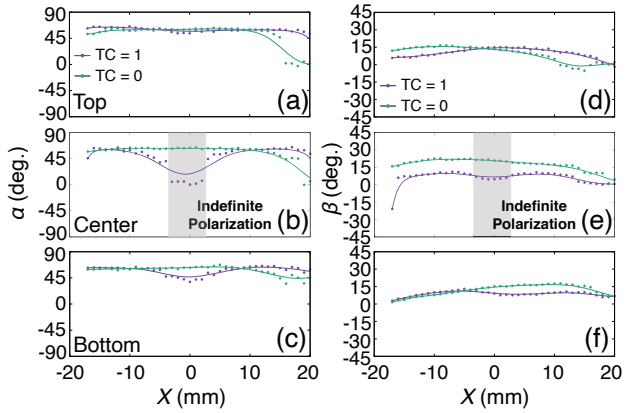

Fig. 9 Variation of polarization parameters based on the position X at each scan path. From (a) to (c) are for α, (d) to (f) are for β. Solid lines are drawn by Bézier interpolation.

(f) are experimental ones. It is easy to see that in the case of TC = 1 at the center path in the experiment, the relative phase is discontinuous across the optical axis. This is a characteristic result where the phase of the vortex beam cannot be defined on the optical axis, and the phase singularity is identified by the heterodyne detection system for the first time. In the calculation, the phase changes 180 degrees when the movable antenna passes through the optical axis. However, the experimental result does not change exactly 180 degrees. The reason is that the center of the antenna does not exactly pass through the center. However, we can estimate that the difference between the center of the antenna and the optical axis is at least 5 mm or less, because the phase discontinuity is not measured when the antenna cross section excludes the optical axis. It is noteworthy that the antenna diameter is 10 mm. Additionally, as can be seen from (d) and (f), an increase or decrease in the relative phase is measured at TC = 1. As shown in Fig. 6 (f), the scan was performed in the X-direction, although the phase of the vortex beam depends on the azimuthal direction. Thus, the relative phase is continuously increasing or decreasing except for the path through the optical axis. On the contrary, there is no change in the relative phase in the X-direction in the case of TC = 0. These experimental results are well compatible with the calculation results.

Finally, Fig. 9 shows variation of the polarization parameters, depending on position of X at each scan path. From (a) to (c) are for α and from (d) to (f) are for β. At the top and bottom paths, there is no change in the polarization parameters in both cases, TC = 1 and TC = 0. However, as can be seen, the polarization parameters drop to zero near the optical axis on the center path at TC = 1. This is because the direction of the electric field vector is distributed in opposite directions across the optical axis, which means that the polarization cannot be defined on the optical axis. On the contrary, when TC = 0, there is no change of the polarization parameters, which are the same as the top and bottom paths. If TC = −1, the same tendency will appear, but the variation of the relative phase, depending on the position of X at the top and bottom lines, will be reversed.

4. Summary

In this study, we measured the one-dimensional phase and polarization structure of the millimeter-wave with a helical wavefront using dual heterodyne detection systems. First, we developed the OMT in the D-band, which is an important millimeter-wave component for measuring a polarization. The OMT had a step taper double-ridge structure, and so the separation performance had approximately 40 dB. The performance was extremely high-performance with a small frequency dependence. Additionally, the D-band polarizer with a rounded shape at the edge of the period groove surface was also developed to generate a beam with an arbitrary polarization state, and its performance test was performed. Therefore, we could obtain a result where the polarization parameters, depending on the set of rotation angles of the polarizers, are almost identical to the calculation result. Based on these results, a vortex beam with an arbitrary polarization was generated, and the cross section of the beam was measured one-dimensionally using the heterodyne detection system. Then, one-dimensional variations in the relative phase and polarization parameters were measured. As a result, it was confirmed that phase discontinuity could be observed, and the polarization parameters also dropped to zero near the optical axis. This means, the optical axis of the vortex beam was a singular point of the phase. Hence, we succeeded in measuring the characteristics of the vortex beam using a heterodyne detection system for the first time.

Acknowledgments

This research was supported by a grant of Joint Research by the National Institutes of Natural Sciences

(NINS) (NINS program no. 01111701), by a grant from The Murata Science Foundation, and by the NIFS grant ULRR033, by NINS program for cross-disciplinary study (grant no. 01311802). The authors would like to thank NIFS technical staff Mr. K. Okada and Mr. S. Kobayashi for designing and manufacturing the OMT.

[1] L. Allen *et al.*, Phys. Rev. A **45**, 8185 (1992).
[2] M. Katoh *et al.*, Phys. Rev. Lett. **118**, 094801 (2017).
[3] M. Katoh *et al.*, Sci. Rep. **7**, 6130 (2017).
[4] Y. Goto *et al.*, J. Adv. Simulat. Sci. Eng. **7**, 1 (2020).
[5] Y. Goto *et al.*, New J. Phys. **23**, 063021 (2021).
[6] T.I. Tsujimura and S. Kubo, Phys. Plasmas **28**, 012502 (2021).
[7] Y. Goto *et al.*, J. Infrared Millim. Terahertz Waves **40**, 943 (2019).
[8] S. Asayama and T. Nakajima, Publ. Astron. Soc. Pac. **125**, 213 (2013).
[9] T. Ii *et al.*, Rev. Sci. Instrum. **86**, 023502 (2015).
[10] K. Nagasaki *et al.*, J. Infrared Millim. Terahertz Waves **20**, 823 (1999).
[11] K. Nagasaki *et al.*, Rev. Sci. Instrum. **66**, 3432 (1995).
[12] Z. Guoqing *et al.*, Plasma Sci. Technol. **11**, 5 (2009).